# Solvation Statics and Dynamics in Electrolyte Solutions. The Ion−Solvent Exchange Model

**R. Argaman, T. Molotsky, and D. Huppert***

*Raymond and Beverly Sackler Faculty of Exact Sciences, School of Chemistry, Tel-Aviv University, Ramat-Aviv 69978, Israel*

*Received: March 9, 2000; In Final Form: May 18, 2000*

We have studied the solvation energetics and dynamics of coumarin 153 in various electrolyte solutions of polar organic solvents. We used a model of two distinct solvates to explain the experimental data. The first distinct solvate was a coumarin dye molecule surrounded by *n* solvent molecules in the first solvation shell. In the second distinct solvate, one of the surrounding solvent molecules was replaced by a cation. Upon photoexcitation of the coumarin dye, an ion−solvent exchange reaction occurred, which was followed by time-resolved fluorescence measurements. The model was successfully applied to coumarin 153 dye in all the solvents used, as well as in a wide range of electrolyte concentrations.

## Introduction

"Solvation dynamics" refers to the rate of solvent reorganization in response to an abrupt change in solute properties. Considerable effort has been devoted to understanding the solvation dynamics of probe molecules in neat solvents.[1−5] However, the solvation of probe molecules in ionic solutions has attracted less attention.[6−14] The solvation dynamics of ions differ from those of solvent molecules. While dynamics in neat solvents primarily involve reorientation of solvent molecules, in ionic solutions ion−probe dynamics arise from translational ion motion as well as from the ion−solvent exchange reaction occurring at the first solvation shell of the probe molecule.

The properties of ionophores, consisting of coumarin 153 and other coumarin dyes linked to several crown ethers, were studied by Valeur and co-workers.[15,16] They found that the photophysical changes, upon complexation with alkali-metal and alkaline-earth-metal cations, can be described in terms of enhancement of the intramolecular charge transfer in the coumarin dye. This is due to the direct interaction between the bound cation and the carbonyl group of the coumarin. The magnitude of the spectroscopic changes is controlled by the charge density of the bound cation. The changes in absorption, as well as emission, spectra were explained in terms of the electrostatic interaction between the cation and the dipole moment of the dye. These authors found in the coumarin 153 absorption spectra shifts of about 1100 and 1500 $cm^{-1}$ and in the emission spectra shifts of about 200 and 700 $cm^{-1}$. The two values refer to the different numbers of oxygen atoms in the crown ethers (four and three atoms, respectively). It was found that there was an isosbestic point in the absorption spectra when salt was added, as well as a satisfactory fit with the 1:1 stoichiometry for the complexation.

Rettig and co-workers[17,18] studied the effects of alkali-metal and alkaline-earth metal cations on the absorption and emission spectra of DMABN attached to crown ethers. They found that upon complexation there was a stabilization of the amine lone pair by an electrostatic interaction with the cation; i.e., cation complexation appeared to reduce or even suppress the charge transfer.

Chapman and Maroncelli[10] measured the statics and dynamics of the salt effects of several probe molecules in electrolyte solutions. They used a number of electrolytes and several organic solvents. Their experimental results agree qualitatively with our basic findings.[6−8] They proposed a solvation model based on equilibria among distinct solvates, characterized by the number of cations in the first solvation shell of the probe. They pointed out that, in the case of a model of distinct solvates, it might be preferable to measure the spectral kinetics in a manner directly related to the growth and decay of these distinct species.

In a previous study,[14] we measured the solvation dynamics of coumarin 153 in an ionic solution of a medium-polarity liquid—butyl acetate—and used a model of distinct solvates[10] to describe the experimental results. In our model, the main ion contribution to the solvation energy of a probe molecule in both the ground and excited states can be described as an ion−solvent exchange reaction:

$$PS_n + I \xrightarrow{k_D} PS_{n-1}I + S$$

where $PS_n$ denotes a probe molecule surrounded by *n* solvent molecules in the first solvation shell, I is an ion replacing a solvent molecule, producing a probe molecule with one cation located in the first solvation shell, denoted as $PS_{n-1}I$. We used a diffusive chemical reaction model[19,20] to describe the dynamics involved in ionic solvation of excited probe molecules. This model leads to a time-dependent rate constant, $k(t)$, and accounts for the viscosity dependence of the solvation dynamics. The results of absorption, steady-state emission, and time-resolved emission spectroscopy of C153 in ionic solutions can be explained by Scheme 1. The two solvates $P^0S_n$ and $P^0S_{n-1}I$ are in equilibrium in the ground state. Upon photon excitation, both ground-state species can be directly excited. For coumarin 153, the excited-state equilibrium constant, $K_{eq}^1$, is larger than that of the ground state, $K_{eq}^0$, $K_{eq}^1 > K_{eq}^0$, and therefore the excited-state exchange reaction can be followed by time-resolved emission.

At high salt concentrations (>0.5 M), we found a systematic mismatch between the specific ion exchange model and the experimental results. The experimental absorption band shifted more to the red than predicted by the model. To account for the additional red shift, we examined two plausible contributions to the solvation energy: (1) We extended the distinct solvate

10.1021/jp000917k CCC: $19.00 
Published on Web 08/08/2000

**SCHEME 1**

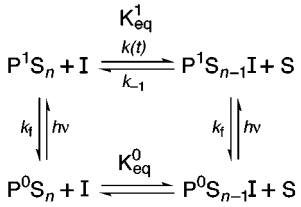


model and incorporated a solvate with two ions into the first solvation shell ($PS_{n-1}I + I \rightarrow PS_{n-2} + S$), and (2) we accounted for the nonspecific contribution of the outer ions to the solvation of the coumarin in the framework of the ionic atmosphere model. We found the second contribution to be much more satisfying to fit our experimental data.

In this study, we apply the extended model to coumarin 153/$LiClO_4$ solutions of two other solvents: ethyl acetate, which differs from butyl acetate in its polarity and viscosity in a minor way, and a small polyether, tetraethylene glycol dimethyl ether (PEG4), with a larger polarity and viscosity (which is about 5 times the viscosity of the two other solvents). Our aim is to find whether we can analyze the solvation dynamics of these two solvents using the model we applied for butyl acetate and, if so, whether we can say something about the differences in solvation between the acetates and the short polymer. Time-resolved fluorescence measurements provide the data for the evaluation of the dynamics of the solvation processes.

## Experimental Section

Time-resolved fluorescence was detected using a time-correlated single-photon-counting (TCSPC) technique. As a sample excitation source, we used a CW mode-locked Nd:YAG-pumped dye laser (Coherent Nd:YAG Antares and a cavity dumped 702 dye laser), which provided a high repetition rate of short pulses (2 ps at full width at half-maximum (fwhm)). The TCSPC detection system is based on a multichannel plate Hamamatsu 3809 photomultiplier and a Tennelec 864 TAC and 454 discriminator. A personal computer was used as a multichannel analyzer and for data storage and processing. The overall instrumental response was about 50 ps (fwhm). Measurements were taken at 20 ns full scale. The samples were excited at 300 nm (the second harmonic of the Rhodamine 6G dye laser). At this wavelength, a sample is excited to $S_2$, the second excited electronic state. The transition dipole moment $S_0 \rightarrow S_2$ is perpendicular to $S_0 \rightarrow S_1$. Therefore, a polarizer set at an angle complementary to the "magic angle" was placed in the fluorescence collection system.

Coumarin 153 (C153) was purchased from Exciton. Butyl acetate (BuOAc), puriss grade, was purchased from Fluka; ethyl acetate (EtOAc), AR, was purchased from Merck; and tetraethylene glycol dimethyl ether (PEG4) was purchased from Aldrich. All chemicals were used without further purification. Steady-state fluorescence spectra of the samples were recorded on an SLM-Aminco-Bowman 2 luminescence spectrometer and corrected according to manufacturer specifications. All experiments were performed at room temperature (24 ± 2 °C).

## Results

**Absorption Spectra of C153 in Electrolyte Solutions.** Figure 1 shows the absorption spectra of C153 in PEG4 solutions containing various concentrations of $LiClO_4$. The absorption spectrum undergoes a red shift of ~450 $cm^{-1}$ from neat solvent to 1 M electrolyte solution. Ethyl acetate and butyl acetate solutions show the same trend, where the maximum red shifts observed (0−1 M) are ~670 and ~780 $cm^{-1}$, respectively. The absorption spectral properties of the three solvents are summarized in Table 1. The absorption spectra undergo changes in shape, width, and height (not just peak position) as the salt concentrations increase. See Table 2 for the characteristic parameters of a single log-normal fit of the absorption spectra of C153 in ethyl acetate, going from a neat solvent to a 1 M $LiClO_4$ solution. The asymmetry parameter and the peak height decrease and the width increases as the electrolyte concentration increases. Note that, for PEG4, the changes in the asymmetry

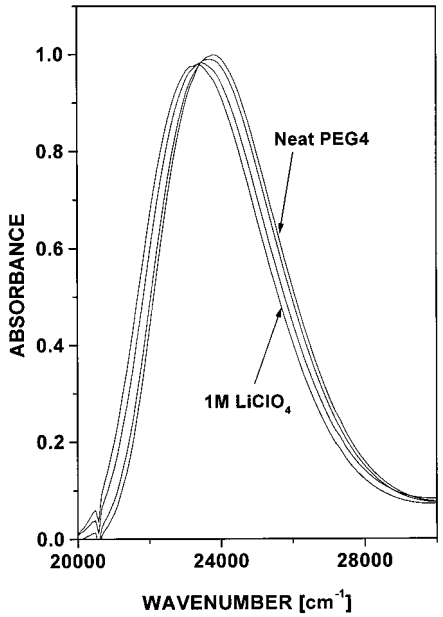


**Figure 1.** Absorption spectra of C153 in PEG4 with various amounts of $LiClO_4$. Right to left: neat PEG4 and solutions with 0.1, 0.5, and 1 M $LiClO_4$.

**TABLE 1: Absorption and Emission Properties of C153 in Various Solvents**

| solvent[a] | $\pi^*$ [b] | $\nu_{abs}$,[c] $cm^{-1}$ | $\Delta\nu_{abs}$,[d] $cm^{-1}$ | $\nu_{em}$,[c] $cm^{-1}$ | $\Delta\nu_{em}$,[d] $cm^{-1}$ |
|---|---|---|---|---|---|
| BuOAc | 0.43 | 24 180 | 782 | 20 190 | 1448 |
| EtOAc | 0.45 | 24 135 | 672 | 20 060 | 1424 |
| PEG4 | 0.56 | 23 750 | 454 | 19 790 | 808 |

[a] Solvents: butyl acetate, BuOAc; ethyl acetate, EtOAc; tetraethylene glycol dimethyl ether, PEG4. [b] The $\pi^*$ value for ethyl acetate was taken from ref 30, and those for the two other solvents were calculated from linear plots of the absorption or the emission maxima of the two solvents versus the known $\pi^*$ values (taken from ref 30) of various solvents.[c] $\nu$ is the band maximum position of the absorption ($\nu_{abs}$) or the emission ($\nu_{em}$) spectrum of the pure solvent. [d] $\Delta\nu$, for the absorption or the emission, is the shift of the respective spectrum from the neat solvent to 1 M $LiClO_4$ solution.

**TABLE 2: Characteristic Parameters for a Single Log-Normal Fit of the Absorption Band of C153 in Ethyl Acetate with $LiClO_4$[a]**

| concn, M | $h$ | $\gamma$ | $\nu_p$, $cm^{-1}$ | $\Delta$, $cm^{-1}$ |
|---|---|---|---|---|
| 0 | 1.015 | 0.356 | 24 135 | 3715 |
| 0.05 | 1.004 | 0.353 | 24 087 | 3722 |
| 0.1 | 0.99 | 0.34 | 24 048 | 3736 |
| 0.35 | 0.975 | 0.325 | 23 858 | 3790 |
| 0.5 | 0.964 | 0.312 | 23 753 | 3823 |
| 0.6 | 0.954 | 0.31 | 23 690 | 3833 |
| 0.8 | 0.939 | 0.3 | 23 573 | 3840 |
| 1 | 0.9 | 0.27 | 23 463 | 3851 |

[a] $h$ is the height of the peak maximum, $\gamma$ is the asymmetry of the peak, $\nu_p$ is the location of the peak maximum, and $\Delta$ is the peak width.

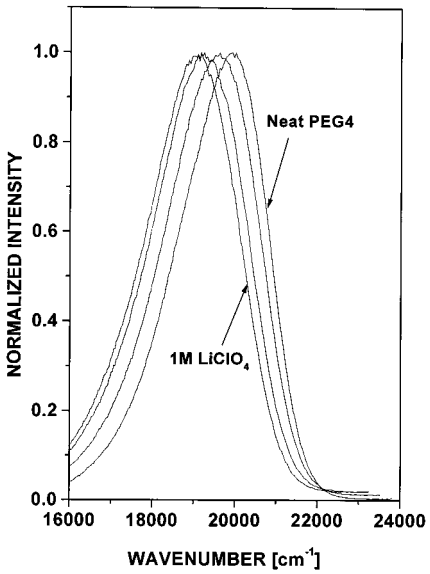


**Figure 2.** Fluorescence spectra of C153 in PEG4 with $LiClO_4$. Right to left: neat PEG4 and solutions with 0.1, 0.5, and 1 M $LiClO_4$. Excitation wavelengths are at the absorption maxima.

**TABLE 3: Characteristic Parameters for a Single Log-Normal Fit of the Emission Band of C153 in PEG4 with $LiClO_4$[a]**

| concn, M | $\gamma$ | $\nu_p$, $cm^{-1}$ | $\Delta$, $cm^{-1}$ |
|---|---|---|---|
| 0 | −0.323 | 19 790 | 2671 |
| 0.01 | −0.324 | 19 730 | 2722 |
| 0.05 | −0.311 | 19 571 | 2844 |
| 0.1 | −0.299 | 19 442 | 2864 |
| 0.2 | −0.284 | 19 321 | 2920 |
| 0.35 | −0.282 | 19 202 | 2929 |
| 0.5 | −0.282 | 19 119 | 2938 |

[a] The excitation wavelength was at the absorption band maximum. $\gamma$ is the asymmetry of the peak, $\nu_p$ is the location of the peak maximum, and $\Delta$ is the peak width. The spectra were normalized to their maxima.

and width are smaller (for reasons that will be discussed in the next section).

**Emission Spectra of C153 in Electrolyte Solutions.** The emission spectra of C153 in neat solvents each show a Stokes shift which is about twice the red shift observed in their absorption spectra. This phenomenon is explained by a large increase of the dipole moment of C153 from a ground-state value of 6.5 D to 14.2 D in the excited state. Figure 2 shows the normalized fluorescence spectra of C153 in PEG4 containing $LiClO_4$. The spectra at a particular concentration of $LiClO_4$ for all the three solvents each show a red shift which is about twice that of the absorption spectrum of each solvent, respectively (see Table 1). Table 3 shows the characteristic parameters of a single log-normal fit of the emission spectra of C153 in PEG4 at several electrolyte concentrations, from neat solvent to 0.5 M $LiClO_4$ solution. These spectra were excited at the absorption band maximum. In addition to the shift of the maximum peak to lower energies, the asymmetry parameter and the width increased as the concentration increased. The same trend is also seen for butyl acetate and ethyl acetate. The magnitude of the red shift in the absorption spectra, as well as in the fluorescence spectra, is larger for the acetates. The reason for this is the increased polarity of PEG4 ($\pi^* = 0.56$) compared to that of butyl acetate and ethyl acetate ($\pi^* = 0.43$ and 0.45, respectively).[21] The same trend is also seen, using C102 as the probe molecule and $NaClO_4$ as the electrolyte, in different solvents.[10] When THF ($\pi^* = 0.58$) is used as the solvent, the shift in the absorption spectrum is 930 $cm^{-1}$, while, in DMSO ($\pi^* = 1.0$), the shift is only 110 $cm^{-1}$. The higher the polarity of the neat solvent, the smaller the shift induced by the ions.[10]

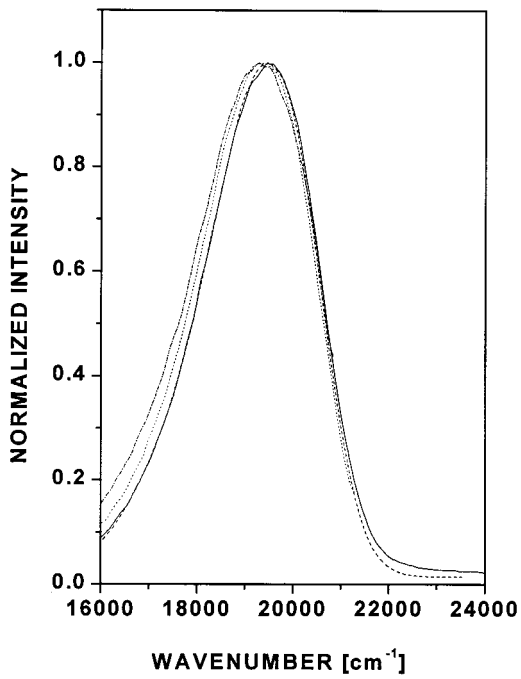


**Figure 3.** Emission spectra of C153 in PEG4 with 0.2 M $LiClO_4$. Excitation wavelengths: (—) 369 nm; (- - -) 422 nm; (···); 466 nm; (— · —) 476 nm.

**Selective Excitation.** Figure 3 shows the emission spectra of C153, in a solution of PEG4 containing 0.2 M $LiClO_4$, excited at four different wavelengths. The emission spectrum shifts to the red and widens when excited at the low-energy end of the absorption spectrum. This shift for PEG4 is about the same as that for ethyl acetate but is much more pronounced for butyl acetate (for butyl acetate, see ref 14). These differences in the emission spectra support the distinctive solvate model, as will be shown and discussed later.

**Time-Resolved Measurements.** Time-resolved emission spectra were measured for the three solvents at various $LiClO_4$ concentrations. A typical plot of the time-resolved emission curves, at several wavelengths, is shown in Figure 4 for PEG4 (containing 0.5 M $LiClO_4$). The emission curves at short times (less than 200 ps) were almost identical to the corresponding curves (the same wavelength) in neat solvents. At times longer than 200 ps, a new decay was seen at short wavelengths ($<$500 nm) and a growth (rising time) at long wavelengths ($>$520 nm). These spectral features are the same for all three solvents. The slow component is attributed to the solvation of coumarin 153 by the salt.

In the next section, we will analyze both the steady-state and time-resolved emission spectra using an extended model which includes the two distinct solvate models and, in addition, a nonspecific contribution to the solvation of the probe by the outer ion atmosphere.

## Data Analysis and Modeling

**The Extended Model.** The extended model is a combination of two different types of contributions to the ion−probe molecule interaction. The first is described by a specific single ion−solvent exchange reaction[10] (described in the Introduction and presented in more detail in a previous paper[14]), and the

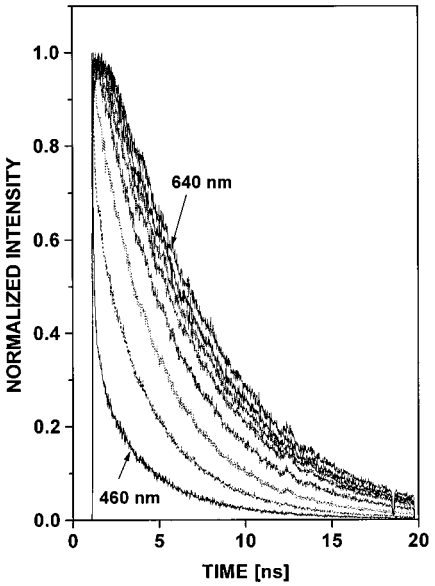


**Figure 4.** Time-resolved emission spectra of C153 in PEG4 with 0.5 M $LiClO_4$ measured at selected wavelengths. Top to bottom: 640, 580, 560, 540, 520, 500, 480, 460 nm.

second is a nonspecific solvation where the ionic atmosphere reaction field affects both the absorption and the emission spectra.[6−9]

The red shift, due to the specific interaction, occurs when an ion replaces one solvent molecule in the first solvation shell of coumarin 153 (according to Scheme 1). The spectral shift in this case is due to the reduction of the $PS_n$ absorption band and the growth of the $PS_{n-1}I$ spectral band.

The nonspecific contribution to the red shift of the absorption spectra is due to the ionic atmosphere interaction with the coumarin molecule dipole. This contribution shifts the absorption bands of both species, $PS_n$ and $PS_{n-1}I$. We assumed that the shift is equal for both species. The best results were obtained when we assumed that the band shift due to the ionic atmosphere contribution is linear with salt concentration. This is represented by the equation $U = d[I]$, where $U$ is the ionic atmosphere contribution to the spectral shift at [I], $d$ is the nonspecific spectral shift (in wavenumbers) at 1 M electrolyte concentration, and [I] is the electrolyte concentration in molar units. We found that $d$ depends on the solvent polarity—the larger the solvent polarity, the smaller the shift.

**Absorption Spectrum.** Figure 5 shows the fits (solid lines) to the experimental absorption spectra of C153 (dashed lines) in three solvents with several salt concentrations, using the extended model. To connect the ground-state equilibrium with an absorption band position and shape (as a function of ion concentration), we assumed that the shape of the spectrum of $P^0S_{n-1}I$ was identical to that of coumarin in the pure solvent except for an overall frequency shift. To generate the line shapes of the absorption spectra of $P^0S_n$ and $P^0S_{n-1}I$, we used a log-normal distribution:

$$I(\nu) = h\begin{cases}\exp[-\ln(2)\{\ln(1+\alpha)/\gamma\}^2] & \alpha > -1 \\ 0 & \alpha \le -1\end{cases} \quad (1)$$

with

$$\alpha \equiv 2\gamma(\nu - \nu_p)/\Delta$$

where $h$ is the peak height, $\nu_p$ the peak frequency, $\gamma$ the asymmetry parameter, and $\Delta$ the band's width. The band shifts in the ground state, between $P^0S_n$ and $P^0S_{n-1}I$, were ~1000 $cm^{-1}$ for both butyl and ethyl acetates and ~600 $cm^{-1}$ for PEG4. The ground-state equilibrium constants were 0.95, 1.12, and 1.8 and the $d$ values (contributions of the outer ionic spheres in 1 M electrolyte) were 450, 250, and 50 $cm^{-1}$, for butyl acetate, ethyl acetate, and PEG4, respectively. As seen in Figure 5, the model calculations are in good agreement with the experimental data.

**Excited-State Dynamics.** When a probe molecule in solution is excited, it experiences a large change in the charge distribution. The dipole moment of C153 increases from 6.5 D[22] in the ground state to 14.2 D[23] in the excited state. The solvent molecules reorient themselves to accommodate the change in the charge distribution of the excited state. Solvent dynamics have been studied extensively and found to be bimodal.[24−26] A

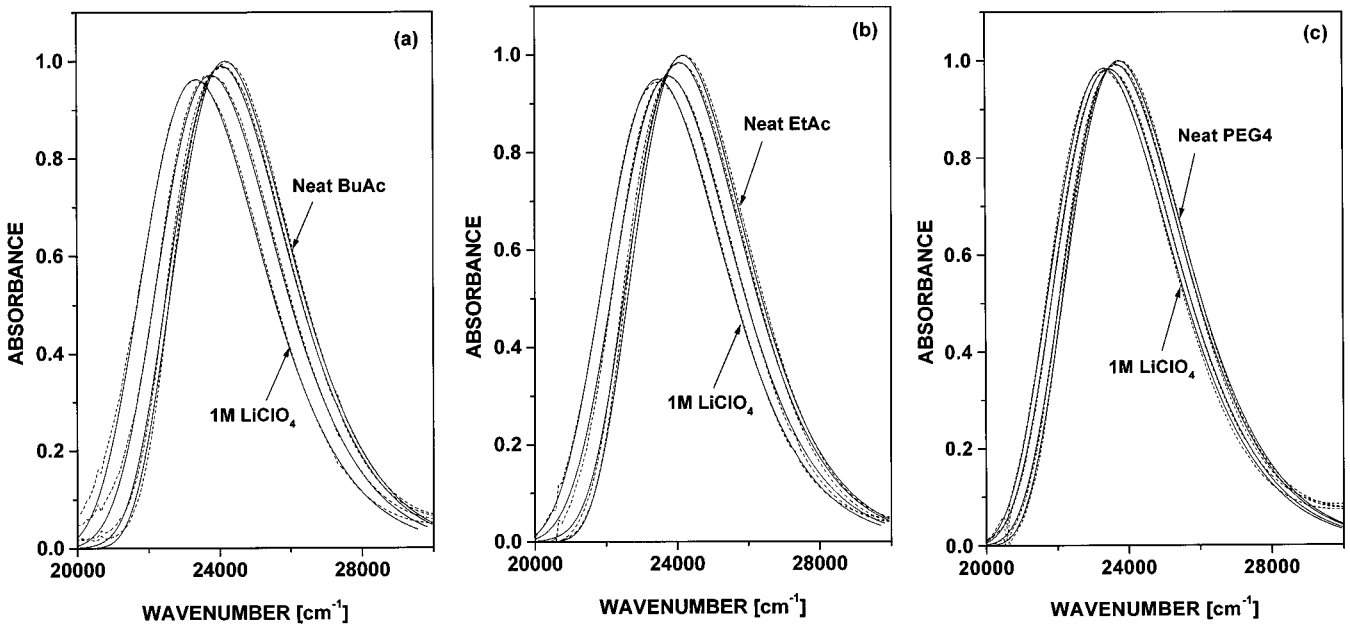


**Figure 5.** Absorption spectra of C153 in (a) butyl acetate, (b) ethyl acetate, and (c) PEG4. Right to left: neat solvent and solutions with 0.1, 0.5, and 1 M $LiClO_4$. Dashed lines are the experimental data, and solid lines are the calculated fits.

**TABLE 4: Parameters for Fitting the Absorption and Emission Spectra to the Two-Species Model**

| | absorption | | | | emission | |
|---|---|---|---|---|---|---|
| solvent | $K^a$ | $d$,[b] cm$^{-1}$ | $\nu_{abs}$,[c] | $\Delta\nu_{abs}$,[d] | $\nu_{em}$,[c] | $\Delta\nu_{em}$,[d] |
| BuOAc | 0.95 | 450 | 24 180 | 900 | 20 190 | 1300 |
| EtOAc | 1.12 | 250 | 24 135 | 970 | 20 060 | 1300 |
| PEG4 | 1.8 | 50 | 23 750 | 600 | 19 790 | 870 |

[a] $K$ is the equilibrium constant for the exchange reaction $PS_n + I \rightarrow PS_{n-1}I$. [b] $d$ is the nonspecific spectral shift at 1 M electrolyte concentration. [c] $\nu_{abs}$ and $\nu_{em}$ are the maxima of the absorption and the emission bands of the $PS_n$ species in cm$^{-1}$ units. [d] $\Delta\nu_{abs}$ and $\Delta\nu_{em}$ are the shifts of the absorption and the emission bands of the $PS_{n-1}I$ species relative to $PS_n$.

large fraction of the change in solvation energy occurs over a very short time span of a few tens of femtoseconds. This component is attributed to the inertial motion of the solvent molecules in the first solvation shell. The fast component is followed by a slower component that decays nonexponentially and is solvent dependent. This component is attributed to the diffusive orientational motion.

When an electrolyte solution is irradiated by a short laser pulse at frequency $\nu$, which coincides with the absorption band of the coumarin dye, both solvates, $P^0S_n$ and $P^0S_{n-1}I$, are excited. The relative probability of a photon being absorbed by $P^0S_{n-1}I$ is given by

$$a(\nu') = \frac{a g_{\nu'}(\nu')}{(1-a) f_{\nu'}(\nu') + a g_{\nu'}(\nu')} \tag{2}$$

where $a$ is the concentration fraction of the $P^0S_{n-1}I$ species in the ground state and $f_{\nu'}(\nu')$ and $g_{\nu'}(\nu')$ are the line shape functions of the ground-state absorptions of $P^0S_n$ and $P^0S_{n-1}I$, respectively.

Immediately after excitation, the solvent in the first solvation shell of the $P^1S_{n-1}I$ species and the solvent molecules in the outer shells experience solvent reorientation to accommodate the excited-state charge distribution of the coumarin. In addition to the solvent solvation energy, an ion situated in the first solvation shell contributes further stabilization which leads to a shift of the $P^1S_{n-1}I$ fluorescence band to lower frequencies relative to the $P^1S_n$ band (for relative values see Table 4). When a photon is absorbed by $P^0S_n$ to create $P^1S_n$, a sudden large increase (of about 8 D) in the dipole moment occurs. This causes a large increase in the equilibrium constant, $K^1 > K^0$ (see Scheme 1). As a consequence, an ion−solvent exchange process takes place at the first solvation layer of the coumarin dye. The following scheme illustrates the dynamics immediately after excitation of the solvate $PS_n$:

$$\begin{array}{ccc} P^1S_n + I & \underset{k_{-1}}{\overset{k_1}{\rightleftharpoons}} & P^1S_{n-1}I + S \\ \downarrow k_f & & \downarrow k_f \end{array}$$

The zeroth-order description of the kinetics of the above scheme is based on the phenomenological rate equations of chemical kinetics. The mathematical solution of the appropriate coupled rate equations is given in ref 27. If $k_1^1 \gg k_{-1}^1$, $k_f$, then the $P^1S_n$ fluorescence intensity decays as a single exponential, while an exponential growth of the fluorescence intensity of $P^1S_{n-1}I$ takes place. The decay rate of the $P^1S_n$ species varies linearly with ion concentration. In the diffusive model, the replacement of a solvent molecule by a cation occurs at a certain rate, whenever I and $P^1S_n$ are in close proximity. As we will show below, if the exchange rate constant is larger than the diffusion rate constant, the dynamics of the reaction is nonexponential. Within the framework of the diffusive model, the well-known way of solving the model is along the lines of the Smoluchowski equation.[19] We used the equation's solution, given in a review by Szabo,[20] to describe the dynamics in the excited state of coumarin 153 dye in an electrolyte solution.

The survival probability of $P^1S_n$ surrounded by an equilibrium distribution of ions, denoted by I, with the initial condition $\rho(0) = 1$, is:

$$\rho(t) = \exp(-c\int_0^t k(t)\,dt) \tag{3}$$

where $c$ is the concentration of the ion and $k(t)$ is the time-dependent rate constant, given by

$$k(t) = \frac{4\pi D a_0 k_0}{k_0 + 4\pi D a_0}\left[1 + \frac{k_0}{4\pi D a_0} e^{\gamma^2 Dt}\,\mathrm{erfc}\{(\gamma^2 Dt)^{1/2}\}\right] \tag{4}$$

where $a_0$ is the contact radius. $\gamma$ is given by

$$\gamma = a_0^{-1}\left(1 + \frac{k_0}{4\pi D a_0}\right) \tag{5}$$

erfc is the complementary error function. $k_0$ is the rate constant of the reaction upon contact. Over long times, the rate constant is independent of time and is given by

$$k = \frac{4\pi D a_0 k_0}{k_0 + 4\pi D a_0} \tag{6}$$

When $k_0 \ll 4\pi D a_0$, $k \approx k_0$ and $k_0$ is the rate constant of the limiting step (which determines the overall rate and not the relative diffusion of the reactants). When $k_0 \gg 4\pi D a_0$, the rate over long times is determined by the diffusion rate constant $k_D = 4\pi D a_0$.

We have found in the past that the inverse of the rate constant ($1/k$) of the salt contribution to solvation of coumarin dyes depends linearly on the solvent viscosity, $\eta$.[6−8] The Stokes−Einstein expression relates $\eta$ to $D$ by

$$D = \frac{kT}{6\pi r \eta} \tag{7}$$

where $r$ is the radius of the diffusing species. For a quantitative description of the time-resolved emission spectrum as well as the steady-state emission spectrum, we used the diffusive reaction rate expressions given by eqs 3 and 4.

**Time-Resolved Fluorescence.** The experimental data analysis reveals that the absorption and emission spectra of $PS_n$ are structureless broad bands having bandwidths of ∼3800 and ∼2750 cm$^{-1}$, respectively. $PS_{n-1}I$ spectra have band shapes similar to those of $PS_n$ spectra; these bands were red-shifted in the absorption as well as the emission spectra, with values given in Table 4. One cannot exclusively excite one species, since the shift between the bands is rather small compared to the width of each band. Therefore, the time-resolved fluorescence signal at a given time, $t$, and frequency, $\nu$, strongly depends on the excitation frequency $\nu'$.

We calculated the signal $I_f(\nu', \nu, t)$ according to

$$I_f(\nu', \nu, t) \propto [(1 - a(\nu'))f_\nu(\nu)\,\rho(t) + a(\nu')\,g_\nu(\nu) + (1 - a(\nu'))(1 - \rho(t))g_\nu(\nu)]e^{-k_f t} \tag{8}$$

where $f_\nu$ and $g_\nu$ are the line shape functions of the $P^1S_n$ and $P^1S_{n-1}I$ luminescences, respectively, and $\rho(t)$ is the survival

**TABLE 5: Relevant Parameters of the Simulation to the Time-Resolved Fluorescence of C153 in Different Solvents with Various $LiClO_4$ Concentrations**

| [$LiClO_4$], M | $\eta$,[a] cP | $a(\nu')$[b] | $10^5D$,[c] $cm^2\ s^{-1}$ | $10^{-9}k_D$ $M^{-1}\ s^{-1}$ | $10^{-9}k_0$,[d] $M^{-1}\ s^{-1}$ | $10^{-9}k$,[d] $M^{-1}\ s^{-1}$ | $\tau_{calc}$,[e] ns | $\tau_{exp}$,[e] ns |
|---|---|---|---|---|---|---|---|---|
| | | | | Ethyl Acetate | | | | |
| 0.05 | 0.51 | 0.06 | 2.0 | 8.77 | 2.8 | 2.12 | 9.4 | 8.64 |
| 0.1 | 0.53 | 0.12 | 1.89 | 8.29 | 2.68 | 2.0 | 4.9 | 4.87 |
| 0.2 | 0.56 | 0.21 | 1.8 | 7.89 | 2.55 | 1.9 | 2.6 | 2.9 |
| 0.35 | 0.59 | 0.3 | 1.7 | 7.46 | 2.4 | 1.82 | 1.57 | 1.65 |
| 0.5 | 0.65 | 0.4 | 1.55 | 6.8 | 2.2 | 1.66 | 1.2 | 1.3 |
| | | | | Butyl Acetate | | | | |
| 0.075 | 0.66 | 0.04 | 1.53 | 6.71 | 2.68 | 1.915 | 6.96 | 7.18 |
| 0.1 | 0.68 | 0.11 | 1.49 | 6.54 | 2.56 | 1.84 | 5.44 | 5.43 |
| 0.2 | 0.73 | 0.2 | 1.39 | 6.1 | 2.38 | 1.7 | 2.94 | 2.9 |
| 0.35 | 0.82 | 0.37 | 1.23 | 5.4 | 2.08 | 1.5 | 1.9 | 1.92 |
| 0.5 | 0.92 | 0.43 | 1.1 | 4.83 | 1.85 | 1.34 | 1.5 | 1.48 |
| | | | | PEG4 | | | | |
| 0.05 | 2.885 | 0.055 | 0.351 | 1.54 | 0.53 | 0.39 | 39 | 40.1 |
| 0.1 | 3.065 | 0.105 | 0.33 | 1.45 | 0.49 | 0.37 | 24.8 | 21.9 |
| 0.2 | 3.39 | 0.19 | 0.298 | 1.31 | 0.4 | 0.3 | 16.3 | 15.03 |
| 0.35 | 4.03 | 0.29 | 0.251 | 1.1 | 0.32 | 0.25 | 11.4 | 12.13 |
| 0.5 | 4.73 | 0.38 | 0.214 | 0.94 | 0.27 | 0.21 | 9.5 | 10.1 |

[a] Viscosities, $\eta$, were deduced from relative viscosity measurements and comparison to known absolute literature values.[31] Measurements were taken at 23 °C. [b] $a(\nu')$ are the relative absorption cross sections of $P^0S_{n-1}I$ irradiated at 300 nm. [c] Diffusion coefficients, $D$, were estimated from the Stokes−Einstein relation and the known viscosities of the solutions. [d] The intrinsic rate constant, $k_0$, was the only adjustable parameter for each solvent. The overall rate constants, $k$, were calculated according to eq 6. [e] $\tau_{calc}$, the relaxation times of the salt, were deduced from $k$, and $\tau_{exp}$ are the times deduced from multiexponential fits of the time-resolved decay curves measured at 470 nm for butyl acetate and ethyl acetate and at 480 nm for PEG4.

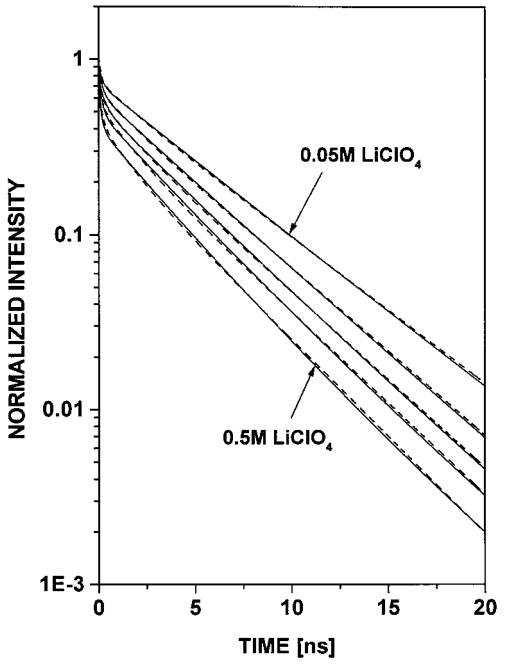


**Figure 6.** Time-resolved emission at 480 nm of C153 in PEG4 with $LiClO_4$. Top to bottom: 0.05, 0.1, 0.2, 0.35, 0.5 M. Dashed lines are experimental data, and solid lines are computer-modeling fits.

probability of $P^1S_n$. The time dependence of $\rho(t)$, due to the ion−solvent exchange reaction, was calculated using eqs 3−6. The first term on the right-hand side of eq 8 is the luminescence intensity, at frequency $\nu$, of $P^1S_n$ excited at frequency $\nu'$. The second term is the luminescence of $P^1S_{n-1}I$ due to direct excitation at frequency $\nu'$. The third term is the luminescence intensity growth of the $P^1S_{n-1}I$ solvate due to the diffusive reaction occurring place in the excited state.

Figure 6 shows the experimental time-resolved emission data measured at 480 nm for C153 in PEG4 (with various salt concentrations), along with the computer fit of the data according to eq 8 (for relative parameters, see Table 5). At this wavelength (470 nm for butyl acetate and ethyl acetate and 480 nm for PEG4), the overlap between the $P^1S_n$ and $P^1S_{n-1}I$ bands is rather small. The luminescence reflects the decay of the $P^1S_n$ population due to the diffusive ligand replacement reaction. The parameters affecting the exchange reaction dynamics are [I], $a_0$, $k_0$, and $D$, where [I] is the $Li^+$ concentration, $a_0$ the contact radius for the reaction, and $k_0$ the intrinsic reaction rate constant at the contact radius. We used a value of $D(\eta[I]) \approx 10^{-5}$ $cm^2\ s^{-1}$ for the diffusion constant of the 0.5 M $LiClO_4$/butyl acetate solution. This value is based on the diffusion coefficient found for the $Li^+$ ion in aqueous solutions.[28] All $D$ values were calculated using this value and corrected to the relative viscosity of the solutions using the Stokes−Einstein relation $D \propto 1/\eta$. We estimated the value of $a_0$ on the basis of the size of the bare coumarin dye (3.8 Å) and our model assumption that the ion−solvent exchange reaction occurs at the interface between the first and second solvation shells. We chose a value of 5.8 Å for the solvated coumarin as a plausible value. Note that, for PEG4, we tried to use different values of $a_0$ for the simulations due to the greater length of this molecule. We found no significant differences for the fit to the experimental data when we used $a_0$ in the range of 5.8 Å $< a_0 <$ 7.8 Å, since $k_D > k_0$ (see below). Taking into account the large flexibility of a polyether, this range for the effective radius is reasonable. $k_D$ is about 3 times larger than $k_0$ for all solvents discussed. Their values are about the same for ethyl acetate and butyl acetate, but those for PEG4 are much smaller. The values of the overall long-time rate constants, $k$, calculated from eq 6, are given in Table 5. From the value of the overall rate constant, we calculated the time constant, $\tau_{calc}$, and compared it with the long-time component observed in the experimental decay curves, $\tau_{exp}$. The calculated values are in very good agreement with the experimental values (see Table 5). Plotting $\tau/\eta$ versus $C^{-1}$ (see Figure 7) gave a linear relation, which indicates that the rate constant for the exchange reaction, $k_0$, changes with the viscosity.

Figure 8 depicts the time-resolved luminescence at selected wavelengths for C153 in PEG4 solution containing 0.5 M $LiClO_4$. At long wavelengths (>520 nm), a time growth of the fluorescence intensity was seen due to the ion−solvent replace-

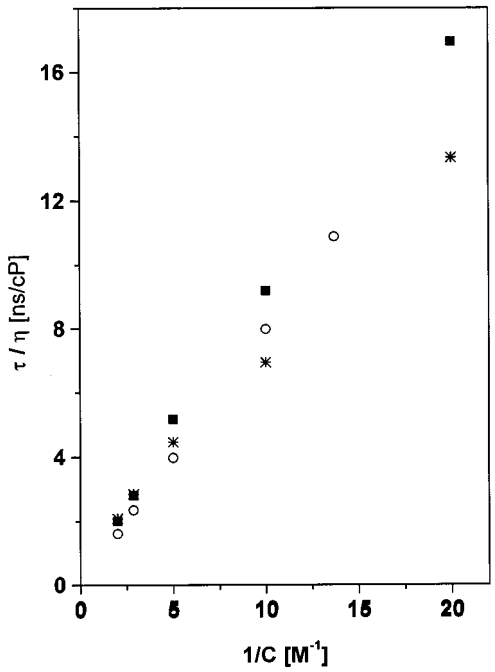


**Figure 7.** $\tau/\eta$ vs the inverse of the concentration of $LiClO_4$: (■) ethyl acetate; (○) butyl acetate; (*) PEG4.

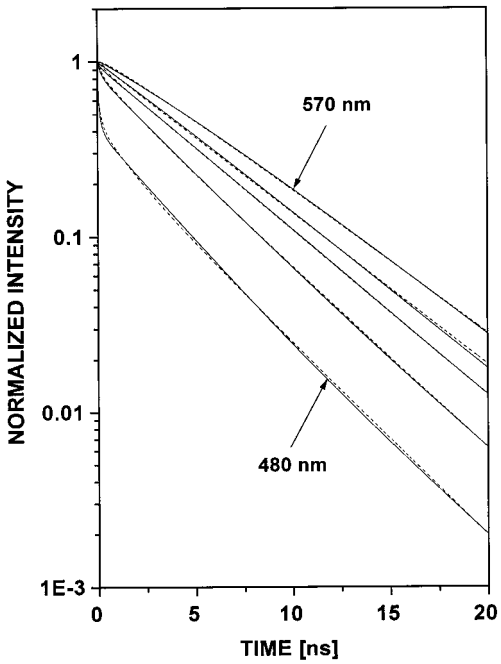


**Figure 8.** Time-resolved luminescence of C153 in PEG4 with 0.5 M $LiClO_4$ at selected wavelengths: (dashed lines) experimental curves; (solid lines) computer modeling fits. Top to bottom: 570, 530, 520, 500, 480 nm.

ment reaction. At these wavelengths, the $P^1S_{n-1}I$ luminescence cross section was larger than that of $P^1S_n$, since the band maximum of $P^1S_{n-1}I$ was located at ~530 nm (for all solvents), while that of $P^1S_n$ was at ~500 nm. There was very good agreement between the calculated (solid lines) and the experimental (dashed lines) fluorescence signals for all solvent and salt concentrations. Due to the large bandwidth and the small shift between $P^0S_n$ and $P^0S_{n-1}$, both solvates are excited by the laser pulse at 300 nm to form $P^1S_n$ and $P^1S_{n-1}$, respectively. The luminescence signals of the component related to direct excitation, at wavelengths >530 nm differed in their relative amplitudes. This component appears instantaneously after excitation, while the fluorescence component due to the exchange reaction has a finite rise time that depends on the electrolyte concentration. Values for the relative fraction of direct excitation for a laser excitation at 300 nm, $a(\nu')$, are given in Table 5.

**Steady-State Fluorescence.** Time integration of the fluorescence expression, given by eq 8, provides the steady-state fluorescence intensity at frequency $\nu$. Sweeping the frequency $\nu$ across the emission frequencies generates the emission spectrum. Figure 9 shows the steady-state experimental spectra as well as the calculated spectra (by integration of eq 8) of coumarin solutions with different electrolyte concentrations of butyl acetate, ethyl acetate, and PEG4. The experimental data fitted the computed integrated fluorescence signals very well.

Another aspect of the model for two discrete solvates, is the dependence of the steady-state fluorescence spectra on the excitation frequency. Figure 10 shows the fit of the model to the steady-state spectra of 0.2 M $LiClO_4$ in PEG4, obtained by excitation at three different wavelengths: at the blue edge of the absorption band (369 nm), at the absorption band maximum (422 nm), and at the red edge excitation (476 nm).

## Discussion

This study consists of steady-state absorption and emission measurements, as well as time-resolved fluorescence measurements, of coumarin 153 in three solvents with different structures, polarities, and viscosities: butyl acetate, ethyl acetate, and PEG4 solutions with $LiClO_4$ as the electrolyte. In previous studies[6−8,12,13] of the electrolyte contribution to the solvation energy of a probe molecule in organic solvents, we adopted a model where a nonspecific interaction of an ionic atmosphere with a probe molecule occurs. It was found that the relaxation times of ionic atmospheres, predicted by the Debye−Falkenhagen (DF) theory, are shorter (by more than 1 order of magnitude) than the observed time-dependent Stokes shift relaxation times. In addition, it was found that the measured solvation energies are larger than those predicted by the DF theory. In contrast to this previous model, Chapman and Maroncelli[10] explained the slow dynamics of the ion contribution to probe solvation by ion−solvent rearrangements in the first solvation shells of the probe molecules. In this study, we adopted their interpretation of the experimental data with some modifications. Moreover, the spectral dynamics occur over longer time periods than the rotations of the probe molecules, implying that the interactions responsible for the shifts must be relatively local. For these reasons, we postulate that ionic solvation dynamics are best viewed as requiring activated exchanges between ions and solvent molecules in the first solvation shells of the probe molecules. We analyzed our data in terms of two distinct solvate configurations, $PS_n$ and $PS_{n-1}I$. $PS_n$ denotes a probe molecule surrounded by $n$ solvent molecules in the first solvation shell, and $PS_{n-1}I$ describes a probe molecule with a single cation incorporated into its first solvation shell. In our case, positive $Li^+$ ions situated close to negative charges of the coumarin dye caused bathochromic shifts in both absorption and emission spectra. These measurements, together with our applied model, lead to some generalizations concerning solvation of highly polar aromatic molecules (C153) in ionic solution.

**Steady-State Measurements.** The main spectroscopic effect of added salt is the induction of a red frequency shift of the probe spectrum. Although there are quantitative differences in the solvents used, the ions affect both the absorption and the emission spectra (with respect to peak positions) of a solvatochromic probe in a similar manner for all the examined systems.

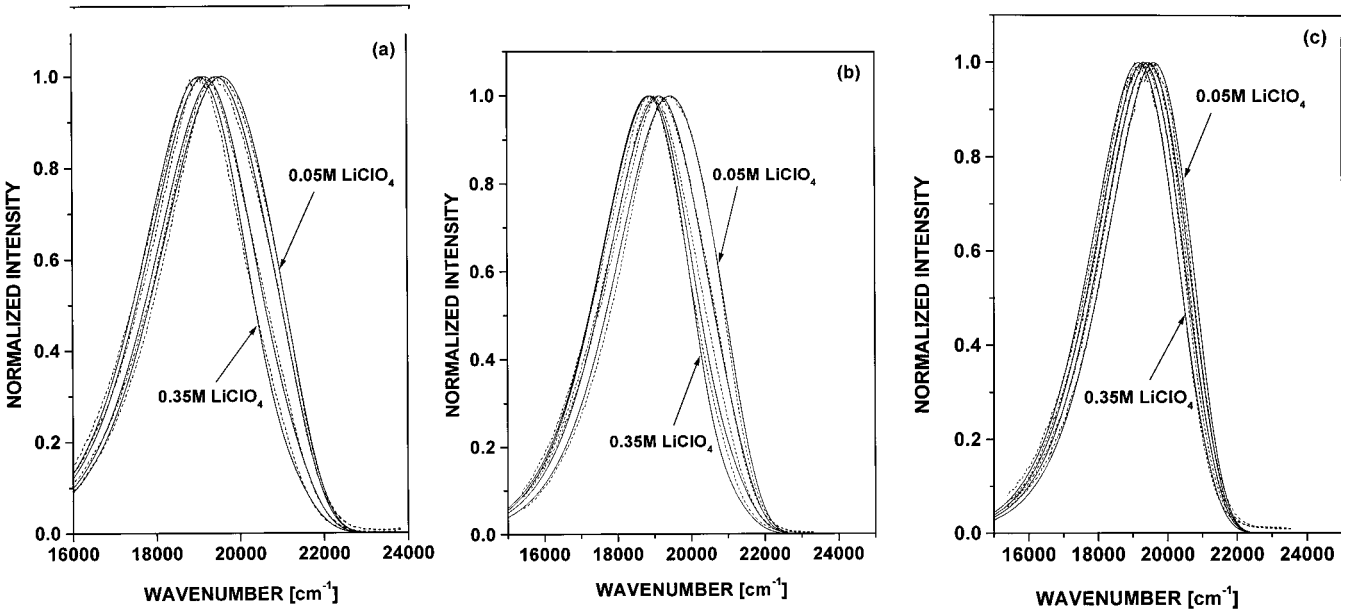


**Figure 9.** Steady-state emission spectra of C153 in (a) butyl acetate, (b) ethyl acetate, and (c) PEG4 solutions of several $LiClO_4$ concentrations: (dashed lines) experimental; (solid lines) calculated. Right to left: 0.05, 0.1, 0.2, and 0.35 M.

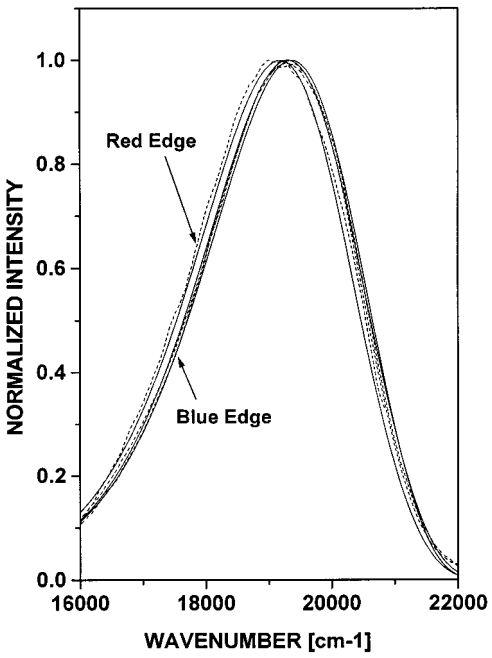


**Figure 10.** Steady-state emission spectra of C153 in PEG4−$LiClO_4$ (0.2 M) solution: (dashed lines) experimental; (solid lines) calculated. Excitations at three different frequencies: at the absorption band blue edge; at the absorption band maximum; at red edge of the absorption band.

According to our previous studies[6−8,12,13] and those of Maroncelli,[10] the same trend is also observed for other salts and probe molecules. The two-solvate model explains the substantial changes in the shapes, widths, and heights of the steady-state spectra as a result of the presence of electrolytes in solution. The structural changes in the absorption spectral bands, as a function of salt concentration, are more pronounced for butyl acetate and ethyl acetate than for PEG4. In all solvents, we find an isosbestic point in each absorption spectrum. As the salt concentration increases, the blue region decreases and the red region increases. For butyl acetate and ethyl acetate, the isosbestic points hold up to a 0.35 M solution. For PEG4, we observe an isosbestic point up to a 1 M electrolyte solution. The fluorescence spectra also change as a function of salt concentration in the cases of butyl acetate, ethyl acetate, and PEG4. Note that the fact that we observe changes in the absorption and emission spectra and isosbestic points in the absorption spectra supports our assumption of the existence of two distinct solvates. In a study by Valeur and co-workers,[15,16] isosbestic points were also observed as a function of electrolyte concentration in the absorption spectra of coumarin dyes linked to crown ethers. The association of ions to crown ethers is large ($K_{eq} \approx 10^5$), and hence the changes in the spectra occurred at low concentrations of $10^{-3}$ M.

In the case of the fluorescence spectra of both acetates, the spectral shift between $PS_n$ and $PS_{n-1}I$ was 1300 $cm^{-1}$. For PEG4, the shift was 900 $cm^{-1}$. The same trend was observed in the absorption spectra, i.e., ∼900 and 600 $cm^{-1}$ for the acetates and PEG4, respectively. This behavior fits the previous findings[6−8,10] that the stronger the solvent−probe interaction, as measured by the probe's absorption frequency in the pure solvent, the smaller the ion-induced shift. We observed red shifts in the absorption spectra of C153 in neat solvents upon going from butyl acetate to ethyl acetate to PEG4. Thus, the solvation energies are in the order PEG4 > EtOAc > BuOAc.

In ionic solutions, the magnitude of the observed spectral shifts is about 10 times larger than those predicted by Debye−Hückel or similar ionic atmosphere theories. The magnitudes of the shifts indicate that a more appropriate picture of ionic solvation involves some sort of ion−probe association, rather than a nonspecific interaction of the probe with a diffusive ionic atmosphere.

**Time-Resolved Fluorescence Measurements.** Time-resolved fluorescence measurements show that the ion dynamics are slow. For $LiClO_4$ 0.5 M in ethyl acetate, butyl acetate, and PEG4 solutions, the solvation times were 1.3, 1.48, and 10.1 ns, respectively. Such slow dynamics further support the idea of ion−probe association. Ultrasonic techniques have been used to study water exchange times for many ions.[29] The exchange times are in the range of a few nanoseconds for monovalent ions, such as the alkali-metal ion used in our study. Petrucci[24] used ultrasonic techniques to measure relaxation times of THF/$LiClO_4$ solutions. A reaction rate constant of $1.6 \times 10^9$ $M^{-1}$

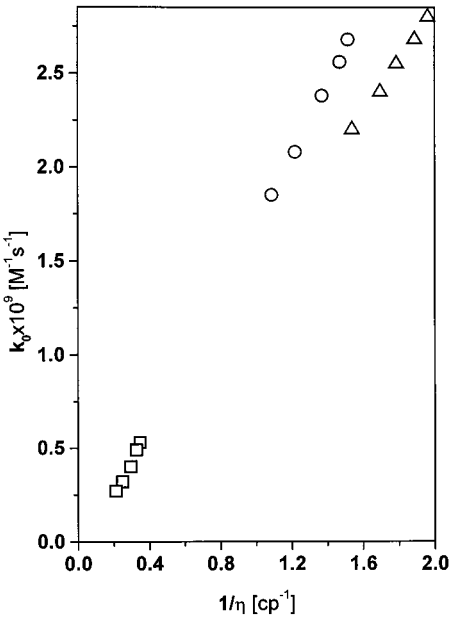


**Figure 11.** Intrinsic rate constants, $k_0$, for different $LiClO_4$ concentrations versus the inverse viscosity in (□) PEG4, (○) butyl acetate, and (△) ethyl acetate.

$s^{-1}$ for $Li^+$ to recombine with a $LiClO_4$ ion pair, to form a triple ion, was calculated from the ultrasonic relaxation time. This rate constant is similar to the rate constants we found in this study for ion solvations in ethyl and butyl acetates.

**Diffusion Formalism.** An important feature in our model is the diffusive nature of the ion−solvent exchange reaction in the first solvation shell of the coumarin dye. The diffusion formalism enables us to account for both the ion transport, to the excited coumarin molecule, and the intrinsic reaction rate.

The time-dependent rate constant, $k(t)$ (eq 4), depends on three parameters: $a_0$, $D$ and $k_0$. We have chosen $a_0 = 5.8$ Å for all solvents, on the basis of the actual size of the coumarin molecule and one solvation shell. $D$ is the mutual diffusion constant: $D = D_{ion} + D_{coumarin}$. The diffusion constants are related to the relative solution viscosity determined for each solution by the relationship $D \propto 1/\eta_{sol}$. The calculated values of $D$ for the solvents used were based on the value of $D$ found for $Li^+$ in water, $D = 1.28 \times 10^{-5}$ $cm^2$ $s^{-1}$,[28] and the known viscosities of the solutions. We calculated diffusion coefficients of $1.55 \times 10^{-5}$, $1.1 \times 10^{-5}$, and $0.214 \times 10^{-5}$ $cm^2$ $s^{-1}$ for ethyl acetate, butyl acetate, and PEG4, respectively.

The only free parameter in our fitting procedure is the intrinsic rate constant, $k_0$. From the computer fit for a particular solvent, we find that $k_0$ has to be adjusted as the concentration increases. It scales nicely with the inverse of the viscosity, $1/\eta(C)$, where $\eta(C)$ is the relative value of $\eta$ as a function of electrolyte concentration. This behavior is shown in Figure 11. From the data analysis, we find that $k_D > k_0$ and that both $k_D$ and $k_0$ depend on the viscosity (which increases with salt concentration). Note that Maroncelli, although neglecting the diffusion part of the dynamics, also pointed out that the rate constant for the exchange reaction scales in a simple manner with solution viscosity. We found that the intrinsic rate constant, for the exchange of a solvent molecule by an ion next to a coumarin dye molecule, depends on the nature of the solvent. The values of $k_0$ for 0.5 M solutions of ethyl acetate, butyl acetate, and PEG4 are $2.2 \times 10^9$, $1.85 \times 10^9$, and $0.27 \times 10^9$ $M^{-1}$ $s^{-1}$, respectively.

From the values of the intrinsic rate and the diffusion rate constants, we calculated the long-time limit rate constants $k$ (see eq 6 and Table 5). We found very good agreement between the calculated rate constants and the experimental values determined from the single-photon-counting experiments.

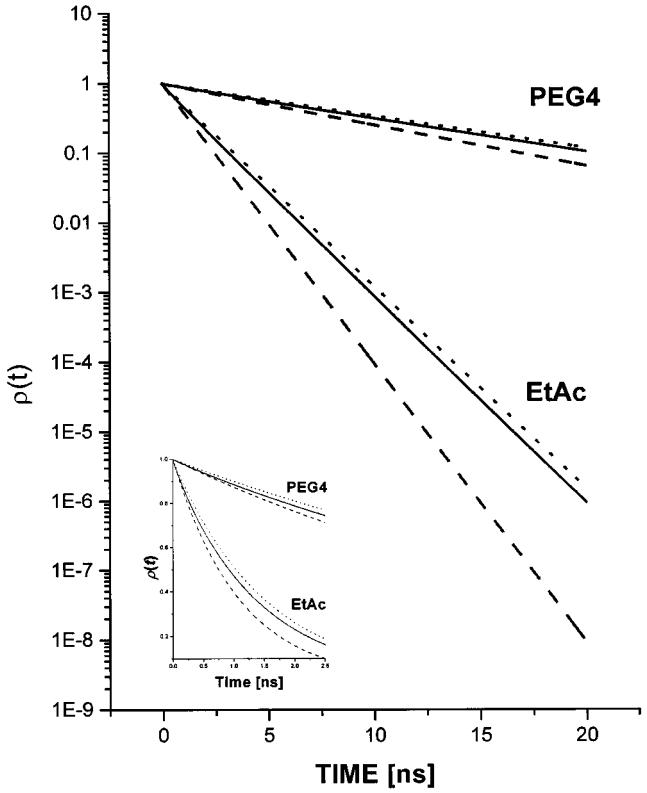


**Figure 12.** Survival probabilities of $P^1S_n$ calculated by eq 3 on a semilog scale as a function of time (solid lines). For comparison are shown the survival probabilities calculated by using the asymptotic long-time expression eq 6 (dotted lines) and the short-time limit $k_0$ (dashed lines). Inset: Time dependence of the survival probabilities on a linear scale at short times.

In eq 4, the time-dependent rate constant assumes the values $k_0$ at the short-time limit and $k_0k_D/(k_0 + k_D)$ at the asymptotic long-time limit. The asymptotic limit is smaller than $k_0$, and thus, the survival probability of excited coumarin given by eq 3 decays nonexponentially. The parameter that determines the extent of nonexponential decay is the ratio $k_0/k_D$: the larger this ratio, the greater the nonexponential behavior. We find that the values of this ratio are 0.3, 0.4, and 0.3 for ethyl acetate, butyl acetate, and PEG4, respectively (see Table 5).

Figure 12 shows, on a semilog scale, the survival probabilities as a function of time for the excited coumarin in the solvents studied. The plots deviate only slightly from those for exponential decay (straight lines). This is expected when $k_0/k_D < 1$, as we found in this study. We are currently studying ion solvation in binary solvent mixtures of water in dioxane. In this case, we found that $k_0 \approx 0.5 \times 10^{10}$ $M^{-1}$ $s^{-1}$, $D \approx 0.4 \times 10^{-5}$ $cm^2$ $s^{-1}$, and $k_D = 2 \times 10^9$ $M^{-1}$ $s^{-1}$. Since the ratio $k_0/k_D$ is 3, we find a large deviation from exponential decay of the ion solvation of the excited-state coumarin in binary solvent mixtures.

**Nonspecific Ion Solvation.** An important finding in this study is the dependence of fluorescence spectra on the excitation frequency. This behavior supports the model of an association equilibrium between cations and the probe solute. Model calculations show that incorporation of a single ion into the first solvation shell of the solute molecule accounts for a major part of the observed spectral shift. We found that the model successfully describes the spectral changes at low salt concen-

trations (up to 0.35 M for the acetates and up to 0.5 M for PEG4) but partially deviates at higher concentrations. The experimental data cannot be explained by the model without invoking additional solvation energy, which can be viewed either as the incorporation of an additional ion or ions into the first solvation shell of the solute molecule or as a nonspecific contribution to the probe solvation by the ionic atmosphere reaction field (which affects both the absorption and emission spectra). These two models were tested by computer fits of the ground-state absorption spectra as a function of electrolyte concentration. We found that an extension of the distinct-solvate model to include $PS_{n-2}I_2$ failed to describe the experimental spectra (in terms of band positions and heights). Much more satisfactory results were obtained when we tested the second model. We assumed that the nonspecific contribution shifts the absorption bands of both species, $PS_n$ and $PS_{n-1}I$, equally. We obtained good results when we presumed that the band shift due to the ionic atmosphere is linear with salt concentration and not square root dependent as expected from the Debye−Hückel theory. For butyl acetate, we obtained a nonspecific contribution of 450 $cm^{-1}$, for ethyl acetate, we obtained 250 $cm^{-1}$, and for PEG4, we obtained 50 $cm^{-1}$, for 1 M electrolyte solutions. We also found the same trend for the specific ion contribution: the larger the solvent polarity, the smaller the spectral shift between $PS_n$ and $PS_{n-1}I$.

## Summary

We measured the steady-state absorption and emission, as well as the time-resolved emission, of coumarin 153 in several organic polar solvents. We analyzed the experimental data in a manner that was directly related to the existence of two distinctive solvates, in both the ground and the excited states. The first solvate was a coumarin molecule surrounded by $n$ solvent molecules in the first solvation shell, and the second solvate included a single cation in the first solvation shell. The dynamics of the ion−solvent exchange reaction was followed, in the first electronic excited state, by time-resolved fluorescence measurements. The exchange reaction was relatively slow and depended on the ion concentration and solvent viscosity. We used diffusion-assisted chemical reaction formalism to describe the excited-state dynamics. We found that the intrinsic rate constant, $k_0$, is about 3 times smaller than the diffusion-limited rate constant, $k_D$. In this case, the asymptotic rate constant $k \approx k_0$. We also found that $k_0$ depends on the solvent viscosity. For moderately polar solvents (ethyl and butyl acetates) at high salt concentrations ($C > 0.35$ M), we found that the model failed to describe quantitatively the changes in the absorption spectra. To account for the slight difference between the calculated and experimental spectra, we invoked a nonspecific contribution to the spectrum red shift from the outer-sphere ions.

**Acknowledgment.** This work was supported by a grant from the James Franck Binational German-Israeli Program for the study of laser−matter interactions.

## References and Notes

(1) Fleming, G. R.; Cho, M. *Annu. Rev. Phys. Chem.* **1996**, *47*, 109.
(2) Reynolds, L.; Gardecki, J. A.; Frankland, S. J. V.; Horng, M. L.; Maroncelli, M. *J. Phys. Chem.* **1996**, *100*, 10337.
(3) Maroncelli, M. *J. Mol. Liq.* **1993**, *57*, 1.
(4) Horng, M. L.; Gardecki, J.; Papazyan, A.; Maroncelli, M. *J. Phys. Chem.* **1995**, *99*, 17311.
(5) Jarzeba, W.; Walker, G. C.; Johnson, A. E.; Barbara, P. F. *Chem. Phys.* **1991**, *152*, 57.
(6) Huppert, D.; Ittah, V.; Kosower, E. M. *Chem. Phys. Lett.* **1989**, *159*, 267.
(7) Huppert, D.; Ittah, V. In *Perspectives in Photosynthesis*; Jortner, J., Pullman, B., Eds.; Kluwer: Dordrecht, The Netherlands, 1990; pp 301−316.
(8) Ittah, V.; Huppert, D. *Chem. Phys. Lett.* **1990**, *173*, 496.
(9) van der Zwan, G.; Hynes, J. T. *Chem Phys.* **1991**, *152*, 169.
(10) Chapman, C. F.; Maroncelli, M. *J. Phys. Chem.* **1991**, *95*, 9095.
(11) Neria, E.; Nitzan, A. *J. Chem. Phys.* **1994**, *100*, 3855.
(12) Bart, E.; Huppert, D. *Chem. Phys. Lett.* **1992**, *195*, 37.
(13) Bart, E.; Meltsin, A.; Huppert, D. *J. Phys. Chem.* **1994**, *98*, 10819.
(14) Argaman, R.; Huppert, D. *J. Phys. Chem. B* **2000**, *104*, 1338.
(15) Bourson, J.; Pouget, J.; Valeur, B. *J. Phys. Chem.* **1993**, *97*, 4552.
(16) Habib Jiwan, J.-L.; Branger, C.; Soumillion, J.-Ph.; Valeur, B. *J. Photochem. Photobiol. A* **1998**, *116*, 127.
(17) Letard, J.-F.; Delmond, S.; Lapouyade, R.; Braun, D.; Rettig, W.; Kreissler, M. *Recl. Trav. Chim. Pays-Bas* **1995**, *114*, 517.
(18) Braun, D.; Rettig, W.; Delmond, S.; Letard, J.-F.; Lapouyade, R. *J. Phys. Chem. A* **1997**, *101*, 6836.
(19) Smoluchowski, M. Z. *Phys. Chem.* **1917**, *92*, 129.
(20) Szabo, A. *J. Phys. Chem.* **1989**, *93*, 6929.
(21) Kamlet, M. J.; Abboud, J. L. M.; Abraham, M. H. *J. Org. Chem.* **1983**, *48*, 2887.
(22) Moyland, C. R. *J. Phys. Chem.* **1994**, *98*, 13513.
(23) Heitele, H. *Angew. Chem., Int. Ed. Engl.* **1993**, *32*, 359.
(24) Passino, S. A.; Nagasawa, Y.; Fleming, G. R. *J. Chem. Phys.* **1997**, *107*, 6094.
(25) Nibbering, E. T. J.; Wiersma, D. A.; Duppen, K. *Chem. Phys.* **1994**, *183*, 167.
(26) Zolotov, B.; Gan, A.; Fainberg, B. D.; Huppert, D. *J. Lumin.* **1997**, *72−74*, 842.
(27) Ireland, J. F.; Wyatt, P. A. H. *Adv. Phys. Org. Chem.* **1976**, *12*, 131.
(28) Bockris, J. O'M.; Reddy, A. K. N. *Modern Electrochemistry*; Plenum Press: New York, 1970; Vol. 1.
(29) Eigen, M.; Tamm, K. Z. *Elektrochem.* **1962**, *66*, 93.
(30) Laurence, C.; Nicolet, P.; Dalati, M. T. *J. Phys. Chem.* **1994**, *98*, 5807.
(31) Weast, R. C. *CRC Handbook of Chemistry and Physics*, 66th ed.; CRC Press: Boca Raton, FL, 1986.